JACS
JOURNAL OF THE AMERICAN CHEMICAL SOCIETY
Article
Cite This: J. Am. Chem. Soc. 2019, 141, 15338−15347
pubs.acs.org/JACS

Controlling O_2 Reactivity in Synthetic Analogues of [NiFeS]- and [NiFeSe]-Hydrogenase Active Sites

Xuemei Yang, Lindy C. Elrod, Trung Le, Valeria S. Vega, Haley Naumann, Yohannes Rezenom, Joseph H. Reibenspies, Michael B. Hall, and Marcetta Y. Darensbourg*

Department of Chemistry, Texas A&M University, College Station, Texas 77843, United States

Supporting Information

ABSTRACT: Strategies for limiting, or reversing, the degradation of air-sensitive, base metal catalysts for the hydrogen evolution/oxidation reaction on contact with adventitious O_2 are guided by nature's design of hydrogenase active sites. The affinity of oxygen for sulfur and selenium, in [NiFeS]- and [NiFeSe]-H_2ase, yields oxygenated chalcogens under aerobic conditions, and delays irreversible oxygen damage at the metals by maintaining the NiFe core structures. To identify the controlling features of S-site oxygen uptake, related **Ni**(μ-E_{PhX})(μ-S'_{N2})**Fe** (E = S or Se, **Fe** = (η^5-C_5H_5)Fe^{II}(CO)) complexes were electronically tuned by the para-substituent on μ-EPhX (X = CF_3, Cl, H, OMe, NMe_2) and compared in aspects of communication between Ni and Fe. Both single and double O atom uptake at the chalcogens led to the conversion of the four-membered ring core, **Ni**(μ-E_{PhX})(μ-S'_{N2})**Fe**, to a five-membered ring Ni−O−E−Fe−S′, where an O atom inserts between E and Ni. In the E = S, X = NMe_2 case, the two-oxygen uptake complex was isolated and characterized as the sulfinato species with the second O of the $O_2S_{Ph\text{-}NMe2}$ unit pointing out of the five-membered Ni−O−S−Fe−S′ ring. Qualitative rates of reaction and ratios of oxygen-uptake products correlate with Hammett parameters of the X substituent on E_{PhX}. Density functional theory computational results support the observed remote effects on the NiFe core reactivity; the more electron-rich sulfurs are more O_2 responsive in the S_{PhX} series; the selenium analogues were even more reactive with O_2. Mass spectral analysis of the sulfinato products using a mixture of $^{18}O_2/^{16}O_2$ suggests a concerted mechanism in O_2 addition. Deoxygenation, by reduction or O atom abstraction reagents, occurs for the 1-O addition complexes, while the 2-O, sulfinato, analogues are inert. The abstraction of oxygen from the 1-O, sulfenato species, is related to oxygen repair in soluble, NAD^+-reducing [NiFe]-H_2ase (Horch, M.; Lauterbach, L.; et al. *J. Am. Chem. Soc.* **2015**, *137*, 2555−2564).

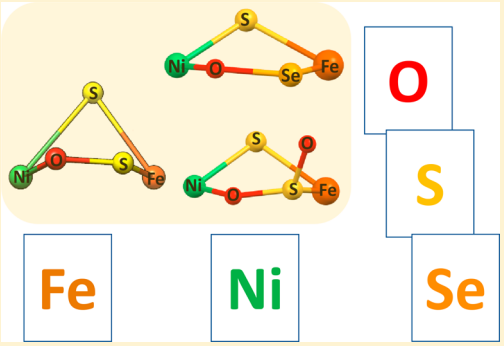

INTRODUCTION

The deleterious effect of O_2 comprises a major challenge in technological development of molecular catalysts for H^+ reduction based on abundant transition metals, needed for sustainable electron conversion to H_2.[1,2] Oxygen as a poison is also well-known to the organisms dependent on hydrogenase enzymes for H_2 production for use as an energy vector in many biological pathways.[3] Evolution over billions of years has developed various strategies for protection from O_2 as a competing, degrading substrate for hydrogenase enzymes as well as possible self-repair mechanisms. Among the different types of hydrogenases, only the [NiFe]-H_2ases provide examples of the capability to operate in the presence of O_2; these are examples of oxygen tolerance.

At least three natural strategies have emerged to protect [NiFe]-H_2ases' active sites from oxygen exposure: (i) a narrow hydrophobic gas channel that hinders diffusion of the bulkier O_2 into the protein-enclosed active site;[4,5] (ii) the presence of an unusual [4Fe-3S] subunit located at the proximal cluster of the O_2-tolerant membrane-bound [NiFe]-H_2ase such as that of MBH from the hyperthermophilic bacterium *Aquifex aeolicus* and *Ralstonia eutropha*, which provides "an electron-rich environment for O_2 detoxification";[6−11] and (iii) the change of a terminal cysteine into selenocysteine in the O_2-resistant [NiFeSe]-H_2ases.[12]

Known to be superior to the all-sulfur analogue, the [NiFeSe]-H_2ase subfamily shows higher activity in HER; reduced inhibition by the product H_2; and, when damaged by adventitious O_2, a more rapid recovery.[13−15] The last feature is likely the greatest contributor to its reputation for O_2 tolerance. The overall protein as well as the active sites of [NiFeS]- and [NiFeSe]-H_2ase are structurally analogous. In the same position as a terminal cysteine sulfur in the former that acts as a proton shuttle to the hydride-loaded NiFe unit, the selenocysteine appears to be poised for the same function in [NiFeSe]-H_2ase.[16] Although SeR^- is a poorer Brønsted−Lowry base than SR^-, and expected to be less prone to proton binding, its larger size renders it a better proton shuttle or directing agent, as it both attracts and releases.[12,17] Nevertheless, its incorporation into synthetic molecular catalysts for proton reduction has been thus far limited.[15,18,19]

Received: July 18, 2019
Published: August 29, 2019

DOI: 10.1021/jacs.9b07448
J. Am. Chem. Soc. 2019, 141, 15338−15347

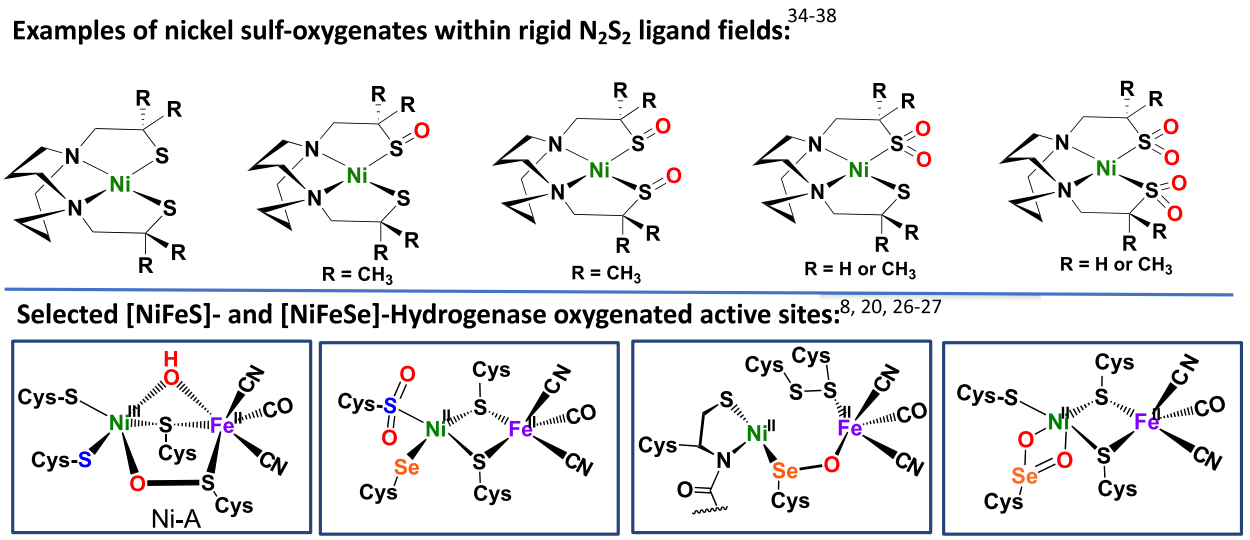

Figure 1. Selected S-oxygenated thiolates in monomeric nickel complexes and examples from crystallography of oxygen-damaged [NiFe]-H_2ase active sites.[8,20,26,27,34−38] Note: the examples of the latter are taken from some 15 to 20 reported structures.

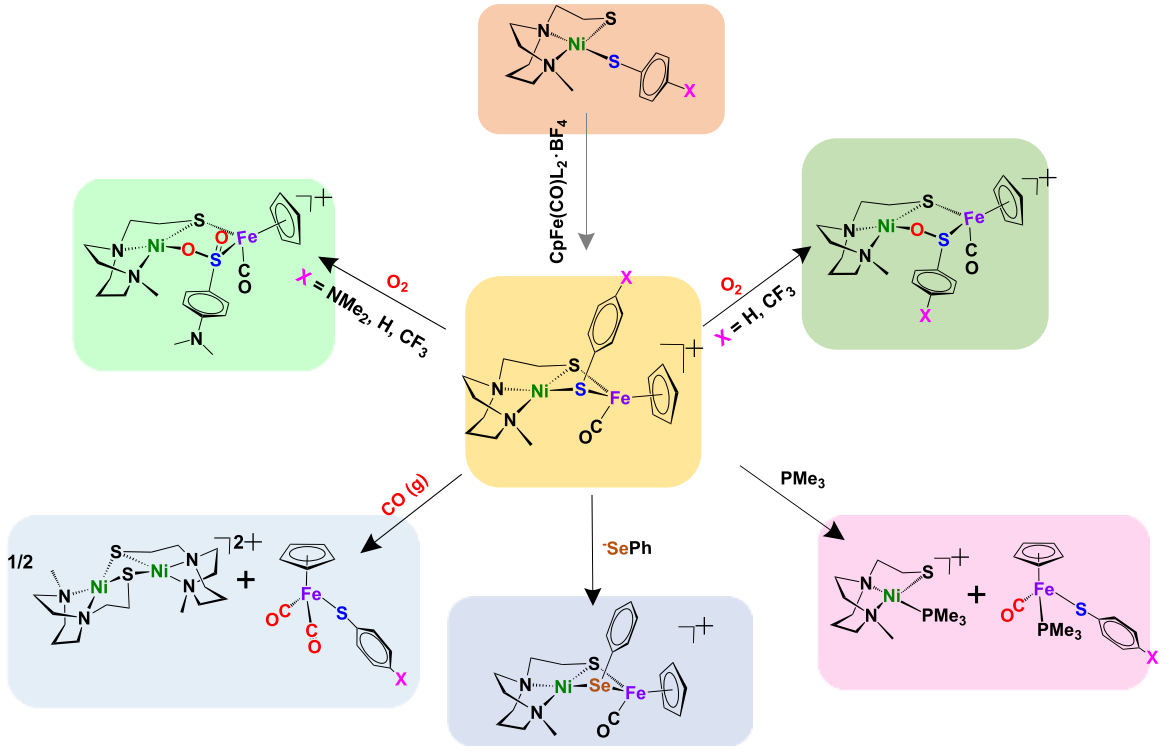

Figure 2. Synthesis of NiFe complexes containing para-substituted arylthiolates and various reactions. L in the $CpFe(CO)L_2^+$ synthon, 12 o'clock arrow position, is CH_3CN as labile ligand. In all products the Ni and Fe are in +2 oxidation states.

Upon exposure of a [NiFeS]-H_2ase to O_2, the active site deactivates to the so-called "Ni-A" (unready) and "Ni-B" (ready) states.[8] The more O_2-tolerant [NiFeS]-H_2ases are known to form "Ni-B" containing a bridging hydroxo ligand between Ni(III) and Fe(II).[20] When electrons and protons from the normal reductive processes are pumped into this ready state, the oxygen is quickly removed (t < 1 min) as H_2O, and catalytic activity is recovered.[2,21−24] However, the "Ni-A" state, also with a hydroxo bridge between Ni(III) and Fe(II) as well as a bridging sulfenate, requires longer times (t > 1 h) to be reactivated, Figure 1.[25] Several structures of these oxygenates have been determined by crystallography, and signals of their presence have long been known from EPR studies, which identified Ni(III) as the redox level in these off-cycle species.[26,27] Studies by Lenz and Zebger et al. show that the conversion of Ni-A to Ni-B in soluble NAD^+-reducing [NiFe] hydrogenase could proceed via oxygenation of the bridging sulfur in Ni−B, whose active site is a structure similar to another unready state found by Fontecilla-Camps.[28,29] It should be pointed out that some 15 to 20 structures with varying degrees of oxygenation at metal or chalcogen in [NiFeS] and [NiFeSe]-H_2ases active sites are found in the protein data bank (PDB) as of this publication. We selected a subset of these to describe in Figure 1. Undoubtedly there will be more in the future.

DOI: 10.1021/jacs.9b07448
J. Am. Chem. Soc. 2019, 141, 15338−15347

In contrast to the [NiFeS]-H_2ase, oxygen-damage of [NiFeSe]-H_2ase results in various O-uptake levels, none of which feature paramagnetic Ni(III); however, selenium and/or sulfur are found oxygenated or oxidized as dichalcogenides in the structures.[30,31] Such oxygenation products of [NiFeSe]-H_2ase, as well as of [NiFeS]-H_2ase active sites, can be interpreted as prevention or protection, avoiding further metal oxidation and degradation of the Ni−Fe core structures in each.[19a,30,31] Reductive repair processes return the enzymes' function in both cases.[32]

Recent reports from Pereira et al. have provided key experiments that constrain the differences in activity of [NiFeSe]- and [NiFeS]-H_2ases to selenium itself rather than any structural changes in the protein.[33] Thus, the simplest explanations for the greater hydrogenase activity and easier reactivation of oxygen-degraded [NiFeSe]-H_2ase as contrasted to the all-sulfur analogue lie in the greater polarizability of selenium, and the weaker Se−O bonds as contrasted to S−O.[17] As such soft descriptions are difficult to quantify, we have pursued relevant structure/function analyses in well-characterized heterobimetallic synthetic analogues containing S and Se. Our ultimate goal is to interpret the clues from synthetic models and from nature that might guide development of robust, oxygen-tolerant, and cheap molecular catalysts for the hydrogen evolution/oxidation reaction.

Examples of S-oxygenated thiolates are plentiful in monomeric complexes containing nickel bound within a rigid tetradentate N_2S_2 ligand field; several examples are displayed in Figure 1.[34−38] In fact, the single oxy-sulfur species, or sulfenate, was used to assemble the first reported biomimetic of S-oxygenated [NiFe]-H_2ase, using $FeBr_2$ as the iron receiver.[39] The synthesis of nickel−iron bimetallic complexes containing both sulfur and selenium, thus providing faithful synthetic analogues of the active sites of [NiFeS]- and [NiFeSe]-H_2ases, represents a considerable challenge.[19,40,41] A strategy found to be successful in the preparation of synthetic analogues of the nickel superoxide dismutase, and for addressing other questions in the bioinorganic chemistry of nickel, is the splitting of dimeric $[NiN_2S]_2^{2+}$ by exogenous thiolates.[30,42,43] Adaptations of this strategy are responsible for the results presented below.

RESULTS AND DISCUSSION

Minimal models of [NiFe]-H_2ase active site core structure are accessed from the cleavage of dimeric $[NiN_2S]_2^{2+}$ complexes by various nucleophiles,[43] including aryl chalcogenides, E_{PhH}^-, E = S and Se.[41] Unlike the stable S-oxygenates described in Figure 1, the resulting monomeric **Ni**$(E_{PhX})(S'_{N2})$ complexes are air-sensitive resulting in degradation. Nevertheless, when combined with $(\eta^5\text{-}C_5H_5)Fe^{II}(CO)(CH_3CN)_2^+$, displacing the CH_3CN labile ligands, the resultant Ni−Fe complexes provide examples of stable products of O_2 uptake, Figure 2. While these models are imperfect structural analogues, our NiFe small molecules offer a paradigm for contrasting S and Se in relevant O_2-addition and repair processes. Moreover, the arylchalcogenides are susceptible to modifications by para-substituents on the arene,[44] giving clues regarding electronic effects operative on oxygen uptake and product distribution. A summary of the reactions explored in this study is found in Figure 2.

Synthesis and Characterizations. The synthetic methods and characterizations (mass spectra, elemental analyses, ^1H NMR spectra, UV and CV spectra, and XRD crystal structures) are further detailed in the Supporting Information. Monomeric **Ni**$(S_{PhH})(S'_{N2})$[41] and *para*-substituted aryl derivatives, **Ni**$(S_{PhX})(S'_{N2})$ (X = CF_3, Cl, H, OMe, NMe_2), were derived from the $[NiN_2S]_2^{2+}$ ([1-(2-mercaptoethyl)-methyl-1,4-diazacycloheptane] nickel(II)) dimer cleaved by the appropriate -S_{PhX}. The **Ni**$(S_{PhX})(S'_{N2})$ complexes readily displaced acetonitrile in the $(\eta^5\text{-}C_5H_5)Fe^{II}(CO)(MeCN)_2^+$ precursor to generate diamagnetic, thermally stable **Ni**$(\mu\text{-}S_{PhX})(\mu\text{-}S'_{N2})$**Fe** (**Fe** = $(\eta^5\text{-}C_5H_5)Fe^{II}(CO)^+$; X = CF_3, Cl, H, OMe, NMe_2) as rudimentary synthetic analogues of the [NiFeS]-H_2ase active sites. Figure 2 summarizes the synthetic scope as well as reactivities explored in this study. The reaction profiles, including O_2 uptake, will be described in separate sections below. A selection of analogous **Ni**$(\mu\text{-}Se_{PhX})(\mu\text{-}S'_{N2})$**Fe** (X = CF_3, H, NMe_2) complexes were similarly prepared and isolated. See the Supporting Information for details.

Molecular Structures. Dark purple, X-ray quality, block crystals of the monomeric **Ni**$(S_{PhX})(S'_{N2})$ complexes were obtained by diethyl ether vapor diffusion into a solution of CH_3CN. The heterobimetallic, cationic **Ni**$(\mu\text{-}S_{PhX})(\mu\text{-}S'_{N2})$**Fe** complexes were isolated as BF_4^- salts and crystallized as dark brown blocks from a pentane-layered CH_2Cl_2 solution at −35 °C. The X substituents on the aryl ring do not substantially modify the structures. The monomeric Ni complexes crystallize in the $P2_1/c$ (X = CF_3), $P\bar{1}$ (X = Cl), and *Pbcn* (X = NMe_2) space groups and feature minimally distorted NiN_2S_2 square planes. The full structural reports of the complexes in Figure 3 are deposited in the Cambridge Database, and selected metric data are tabulated in the Supporting Information (Figure S43).

The **Ni**$(\mu\text{-}S_{PhX})(\mu\text{-}S'_{N2})$**Fe** complex structures feature square planar **Ni**$(S_{PhX})(S'_{N2})$ units connected by chalcogenide bridges

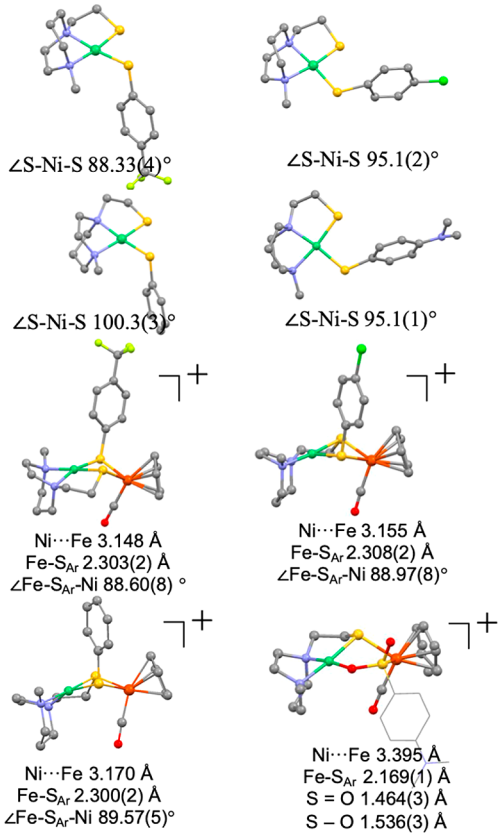

Figure 3. Molecular XRD structures determined for monomeric Ni and for the **Ni**$(\mu\text{-}S_{PhX})(\mu\text{-}S'_{N2})$**Fe** complexes. Full listings of metric data are in the Supporting Information.

DOI: 10.1021/jacs.9b07448
J. Am. Chem. Soc. 2019, 141, 15338−15347

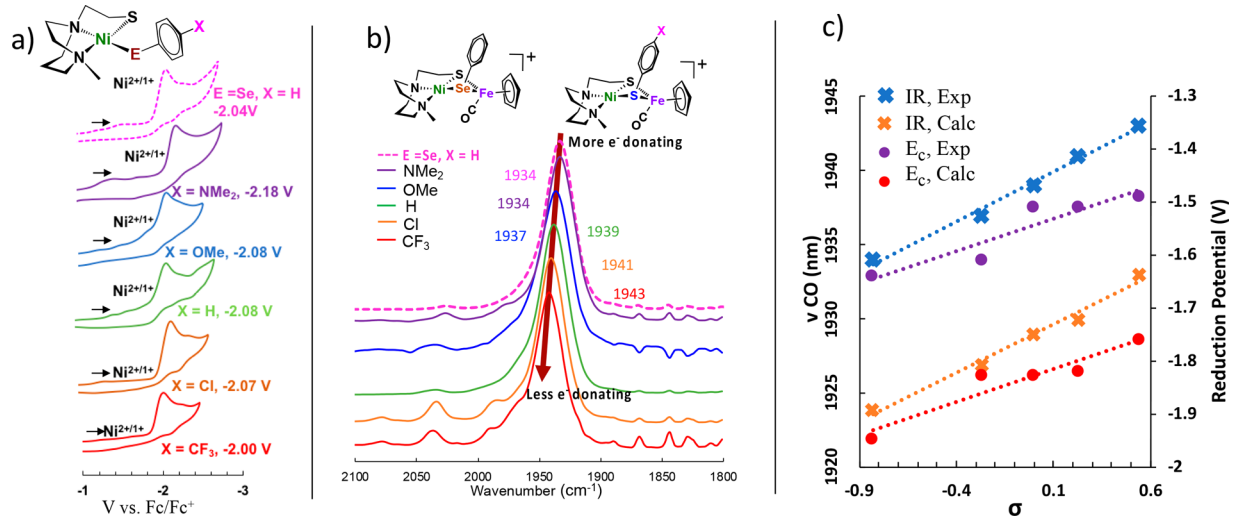

Figure 4. (a) Cyclic voltammograms in E_c region for Ni^{II}/Ni^{I} and monomeric Ni complexes; (b) ν(CO) IR spectra of **Ni**(μ-E_{PhX})(μ-S'_{N2})**Fe**; (c) correlations of Hammett σ parameters with experimental and calculated ν(CO) values and E_c values of Ni^{II}/Ni^{I} in **Ni**(μ-S_{PhX})(μ-S'_{N2})**Fe**.

into the typical piano-stool geometry about the $[(\eta^5\text{-}C_5H_5)Fe(CO)]^+$ unit, resulting in butterfly-like Ni−S−Fe−S′ cores. The hinge angles, defined as the intersection of the best N_2SS' plane with the SS′Fe plane, are in the range of 135−141°. The $Ni^{II}\cdots Fe^{II}$ distances of 3.1−3.2 Å are beyond the possibility of a metal−metal bond. Earlier we reported the XRD structures of the **Ni**(μ-Se_{PhH})(μ-S'_{N2})**Fe** with the $Ni^{II}\cdots Fe^{II}$ distance = 3.253 Å, and the mono-oxy derivative of the phenyl-selenolate. The expanded five-membered metallocycle seen in the latter, has a slightly larger $Ni^{II}\cdots Fe^{II}$ distance, 3.568 Å. In the current study, only the X = NMe_2 derivative provided X-ray quality crystals from reaction of **Ni**(μ-S_{PhX})(μ-S'_{N2})**Fe** with O_2. The structure displays a sulfinate unit in the five-membered Ni−O−S(=O)Fe−S′ ring, with $Ni^{II}\cdots Fe^{II}$ distance = 3.395 Å. In summary, neither the two-oxy or the mono-oxy products show significant modification of the Ni−Fe bimetallic structures.

IR Spectra and Electrochemical Characterizations. Correlations of the Hammett σ_p parameter with ν(CO) IR values and $Ni^{II/I}$ reduction potentials derived from cyclic voltammetry, for the series of NiFe complexes, are presented as plots in Figure 4.[44] Both theoretical (density functional theory (DFT)-derived values) and experimental data of the ν(CO) in **Ni**(μ-S_{PhX})(μ-S'_{N2})**Fe** and $E_{cathode}$ potentials for Ni^{II}/Ni^{I} in monomeric **Ni**(S_{PhX})(μ-S'_{N2}) complexes conform with the Hammett parameters of the X substituents on the -S_{PhX} ligands. Specifically, more electron-donating substituents result in lower ν(CO) values, illustrating electronic communication over five bonds and the influence on π-backbonding from Fe^{II} to the CO. The **Ni**(μ-Se_{PhX})(μ-S'_{N2})**Fe** series shows ν(CO) responses to X similar to the sulfur analogues however moderated in value. Interestingly, the phenyl derivative with the most electron-donating substituent, **Ni**(μ-S_{PhNMe2})(μ-S'_{N2})**Fe**, gives the same ν(CO) value (1934 cm^{-1}) as that found in **Ni**(μ-Se_{PhH})(μ-S'_{N2})**Fe**. There is not such a match in the $Ni^{II/I}$ reduction potential.

Computational Section I. DFT calculations were performed using the TPSSTPSS functional with the 6-311++G(d,p) basis set on the nonmetal atoms and the 6-311+G basis set on nickel and iron in the Gaussian16 suite.[45] The molecular structures from XRD presented above were used as geometric starting points with all other structures made by the appropriate atomic substitutions in the AMPAC Graphical User Interface (AGUI).[46] All structures were optimized in solvent by using the SMD solvation model with acetonitrile as the solvent. Vibrational frequencies were calculated "in solvent", and all species were confirmed to be minimum energy structures by the absence of imaginary frequencies. Standard statistical mechanical and solvation corrections were applied to the electronic energy of the optimized structures to give free energy values (standard states were not converted to mol/L).

The computational methods yielded the structures and energies of the **Ni**(μ-S_{PhX})(μ-S'_{N2})**Fe** complexes as well as their singly and doubly oxygenated forms. These calculations aimed to examine how the properties of the model complexes depended on the chalcogen identity, sulfur vs selenium, and with para-substituents, X, that modified the electron-donating properties of the E-PhX. Our computational method accurately reproduces the trends seen in the experimental data for structures (where available), the trends in ν(CO) IR values (absolute values are underestimated), and the positions of $Ni^{II/I}$ reduction potentials (Figure 4).

Mentioned above, the **Ni**(μ-E_{PhX})(μ-S'_{N2})**Fe** complexes with E = Se, X = H and with E = S, X = NMe_2 display the same ν(CO) values in experiment (1934 cm^{-1}) and from theory (1895 cm^{-1}). These equivalent values indicate that, as relayed by iron to the carbon monoxide ligand, the -Se_{PhH} and the -S_{PhNMe2} are equally strong electron donors. Similarly, the calculated ν(CO) stretch for the singly oxygenated **Ni**(μ-O-μ-Se_{Ph})(μ-S'_{N2})**Fe** (1919 cm^{-1}) is comparable to that of **Ni**(μ−O-S_{PhNMe2})(μ-S'_{N2})**Fe** (1921 cm^{-1}). In contrast with the doubly oxygenated complexes the ν(CO) value calculated for the two-oxy species, the **Ni**(μ-O-(O=)Se_{PhH})(μ-S'_{N2})**Fe** complex (1936 cm^{-1}) is now most similar to the sulfur analogue with the electron withdrawing X = CF_3, i.e., **Ni**(μ-(μ-O-S(=O)$_{PhCF3}$)(μ-S'_{N2})**Fe**. There are minor differences in for the three dioxy selenium species. Table S1 lists ν(CO) values of all species that were derived experimentally and also the DFT calculated values.

Chemical Reactivity. Various chemical reactions of **Ni**(μ-S_{PhX})(μ-S'_{N2})**Fe** complexes are presented in Figure 2. In the **Ni**(μ-S_{PhX})(μ-S'_{N2})**Fe** series, the -Se_{PhH} ligand is found to replace the -S_{PhX} to form **Ni**(μ-Se_{PhH})(μ-S'_{N2})**Fe** in low yield along with degradation products. Under CO(g), the **Ni**(μ-S_{PhX})(μ-S'_{N2}) complexes cleanly convert into dimeric $[NiN_2S]_2^{2+}$ and $(\eta^5\text{-}C_5H_5)Fe(CO)_2S_{PhX}$. With PMe_3, the **Ni**(μ-S_{PhX})(μ-S'_{N2})**Fe** also easily cleaves into two products:

DOI: 10.1021/jacs.9b07448
J. Am. Chem. Soc. 2019, 141, 15338−15347

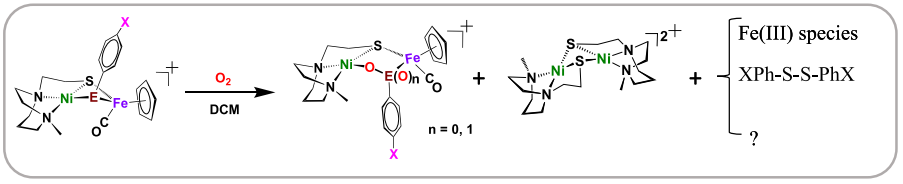

E-X	σ	Reaction time	Main Product	Combined Yield of Oxygenate(s)
S-NMe_2	-0.830	3.5 h	2-Oxy Species	55 %
S-H	0.000	7 h	Mixture (n = 0, 1)	37 %
S-CF_3	+0.540	24 h	Mixture (n = 0, 1)	30 %
Se-NMe_2	-0.830	0.8 h	1-Oxy Species	61 %
Se-H	0.000	2 h	1-Oxy Species	56 %
Se-CF_3	+0.540	3.5 h	Mixture (n = 0, 1)	40 %

Figure 5. Reactions of Ni(μ-E_{PhX})(μ-S_{N2})Fe complexes dissolved in CH_2Cl_2 under 1 atm O_2 at room temperature. Reaction time is defined as that required to reach a plateau of the product ν(CO) band. Attempts to separate or determine the distribution in the mixtures of 1- and two-oxy products were unsuccessful. Components of product mixtures identified by $^+$ESI-mass spectrometry.

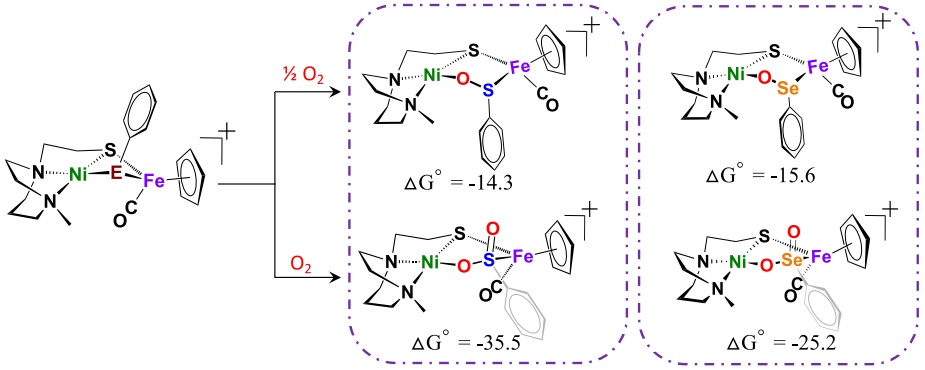

Figure 6. DFT calculated free energy values, $\Delta G°$, for comparison of oxygen-uptake reactions of **Ni**(μ-E_{PhH})(μ-S'_{N2})**Fe** complexes, E = S and Se, in kcal/mol.

Ni(S'_{N2})(PMe_3) and (η^5-C_5H_5)Fe(CO)(PMe_3)S_{PhX}. In summary, (a) the reactivity of **Ni**(μ-S_{PhX})(μ-S'_{N2})**Fe** with the poor nucleophile, CO, is controlled by -S_{PhX} shifting to Fe with concomitant release of $[Ni(S'_{N2})]^+$, readily scavenged by another of itself forming the thermodynamically stable $[NiN_2S]_2^{2+}$; (b) with the good nucleophile, PMe_3, both the Ni and Fe products contain PMe_3. The fact that -S_{PhX} prefers the Fe^{II} rather than Ni^{II} is consistent with the observation of oxygen insertion between Ni and S_{Ph} that leaves the sulfur of -S_{PhX} bound to Fe, *vide infra*.

Reactions with O_2. Three **Ni**(μ-S_{PhX})(μ-S'_{N2})**Fe** and three **Ni**(μ-Se_{PhX})(μ-S'_{N2})**Fe** complexes were selected for studies of O_2 reactivity: X = NMe_2 (most electron-donating); X = H; and X = CF_3 (most electron-withdrawing). Details of the experimental protocol are deposited in the Supporting Information (p S4, Synthesis and Characterization Section). Dichloromethane solutions of the NiFe complexes were sparged with O_2 for 30 min at 22 °C. The reactions were monitored by ν(CO) FTIR spectroscopy until no further changes, followed by Celite filtration and isolation of the S-oxygenated products by solvent removal. Mass spectroscopy ($^+$ESI) was used to identify the components in the product mixture. A summary of results is found in Figure 5. In all cases, the byproducts were the disulfide, XPhS−SPhX, and the dimeric species, $[NiN_2S]_2^{2+}$. The presence of an Fe^{III} species isolated from residual solids was established by addition of aqueous Na^+SCN^- with formation of the blood red $[Fe(SCN)(H_2O)_5]^{2+}$ complex.

Under identical conditions for **Ni**(μ-S_{PhX})(μ-S'_{N2})**Fe** derivatives of three arene substituents, we compared the O_2 reaction times and yields of the principal products. In the case of X = H, 7 h are required to complete the O_2 reaction, yielding a mixture of the mono- and dioxy species with overall yield of 37%.[41] In contrast, when X = CF_3, the reaction required 24 h to maximize the products from the reduced form, with ν(CO) at 1943 cm^{-1}, to oxygenated products (a mixture of one-oxy and two-oxy species) that displayed as an unresolved broad ν(CO) band at 1971 cm^{-1}. The isolated yield was ca. 30%. With the Me_2N substituent, the major product is the dioxy species, isolated in 55% yield after 3.5 h.

For comparison, the **Ni**(μ-Se_{PhH})(μ-S'_{N2})**Fe** completed reaction with O_2 after only 2 h, giving a 56% yield of sulf-oxygenated products predominantly of the mono-oxy type.[41] Modifications using CF_3 and NMe_2 as para-substituents in -Se_{PhX} gave slower (3.5 h) and faster (0.8 h) reactions with O_2, respectively. In summary, while selenium analogues are more reactive than sulfur, both the selenolate and thiolate bridges respond to the X substituent on the aryl groups. The more electron-donating substituent in the aryl-substituted chalcoge-

DOI: 10.1021/jacs.9b07448
J. Am. Chem. Soc. 2019, 141, 15338−15347

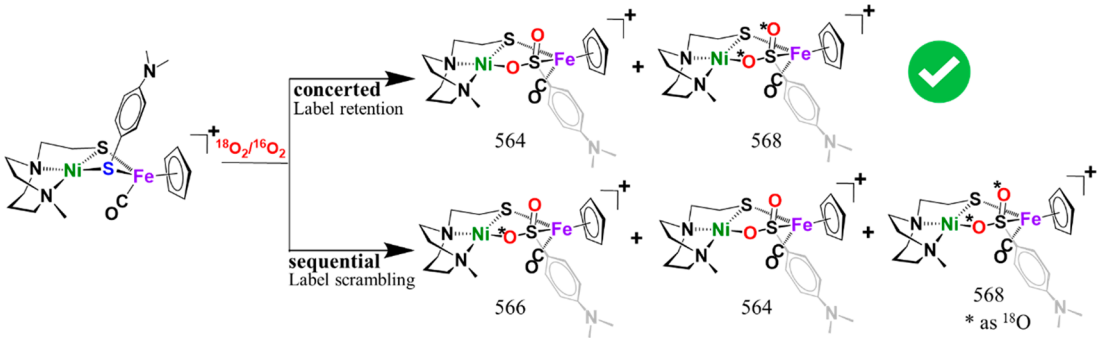

Figure 7. Predicted concerted and sequential mechanisms for the reactions of **Ni**(μ-S_{PhX})(μ-S'_{N2})**Fe** complexes with $^{18}O_2$.

nide ligands, **Ni**(μ-E_{PhX})(μ-S'_{N2})**Fe**, gave greater yields and more rapid E-oxygenation reactions. The reaction time profile is as follows:

$$0.8\ \text{h(SePh-NMe}_2) < 2\ \text{h(SePh-H)} < 3.5\ \text{h(SePh-CF}_3)$$

$$\approx 3.5\ \text{h(SPh-NMe}_2) < 7\ \text{h(SPh-H)} < 24\ \text{h(SPh-CF}_3)$$

The identical ν(CO) absorptions (1934 cm^{-1}) of the **Ni**(μ-Se_{PhH})(μ-S'_{N2})**Fe** and the **Ni**(μ-S_{PhNMe2})(μ-S'_{N2})**Fe** complexes are reasonably connected to their oxygen reactivity, which is significantly greater than the congeners in the series. While the electron density reported by π-back-bonding of iron to CO appears to be the same in the two complexes, a difference exists in reactivity (time to completion) and product distribution. A single O-uptake for **Ni**(μ-Se_{PhH})(μ-S'_{N2})**Fe**) leads to the selenoate, Ni−O−Se−Fe−S′ bridge between Ni and Fe; a two-oxy addition, with production of a bridging sulfinato complex, Ni−O−S(=O)−Fe, is seen for product (>90% of the two-oxy species) from **Ni**(μ-S_{PhNMe2})(μ- S'_{N2})**Fe**.

Computational Section II. The O-uptake distinctions in the Ni−Fe complexes inspired further DFT computations that addressed thermodynamic driving forces for O_2 reactions and the two types of products. Summarized in Figure 6 are free energies, $\Delta G°$, for the sulfur and selenium single oxygenation reactions found to be similar at −14.3 and −15.6 kcal/mol, respectively. The double oxygenation reactions, however, show a greater difference; the $\Delta G°$ in the selenium case is −25.2 kcal/mol, whereas the sulfur case is favored by −35.5 kcal/mol. The selenium two-oxy species is more stable than the one-oxy, but the energy gap between the levels (9.6 kcal/mol) is approximately half as large as the energy gap for the sulfur analogues (21.1 kcal/mol). While the reaction energies indicate in both cases the two-oxy species should be the thermodynamic product, only the sulfur displays the sulfinate. In the absence of a mechanism for the O_2 uptake reaction we suggest possible working hypotheses: (#1) the selenium two-oxy product is less kinetically accessible than the one-oxy product; or (#2) the two-oxy product is formed but the weak terminal Se=O, see below, allows the complex to undergo comproportionation with the mixed chalcogenide precursor to form two equivalents of one-oxy products. This type of reactivity has no direct analog in enzymes due to the enclosed nature of the active site.

Reasonable support for hypothesis #2 is that the difference in the $\Delta G°$ for the two-oxy complexes correlates with the strength of the π bond to the terminal oxygen for sulfur vs selenium. The Natural Bond Orbital (NBO)[47] analysis (second order perturbation) reveals the total stabilization energy coming from interactions of the lone pairs on the terminal oxygen with the chalcogen to be 24.4 kcal/mol for the sulfur and 13.0 kcal/mol for the selenium variant. While the natural atomic orbitals that make up the S=O and Se=O π interaction (details in the SI) appear nearly identical, the greater electronegativity difference for Se and the greater orbital size mismatch for Se results in the weaker π bond with the terminal oxygen as compared to sulfur.

Mechanism of O_2 Addition—Isotopic Labeling. Notably, the addition of O_2 in the case of X = NMe_2 in **Ni**(μ-S_{PhX})(μ-S'_{N2})**Fe**, cleanly yields the two-oxy-sulfur, or sulfinato, complex as the main oxygenate. We addressed the question of concerted addition of the oxygen atoms from one O_2 molecule or stepwise addition from separate O_2 molecules by isotopic labeling/crossover experiments, as shown in Figure 7. A mixture of $^{18}O_2/^{16}O_2$ (in ratio of 38:62) gas was added to a CH_2Cl_2 solution of **Ni**(μ-S_{PhNMe2})(μ-S'_{N2})**Fe** complex, and isolated products were subjected to mass spectrometric analysis in order to determine the isotope distribution in the product sulfinato complex. If a concerted mechanism prevails, the dioxy product should retain the labels of the O_2 substrate; if stepwise addition, there should be evidence of label scrambling, the $^{16}O^{18}O$ sulfinato product. Isotopic bundle analysis finds an isotopomer at the mass peak of 566 m/z, which is distinctive as an indicator for label scrambling. The theoretical distributions in the ion bundle are shown in Figure 8 along with the experimental result for the specific mixture of $^{18}O_2/^{16}O_2$. From the lack of a match of the m/z 566 signal, we conclude that the experimental reaction mixture best fits label retention; i.e., the isotopomeric dioxy products are $Ni^{16}O^{16}O$ SFe and $Ni^{18}O^{18}O$ SFe, and the two

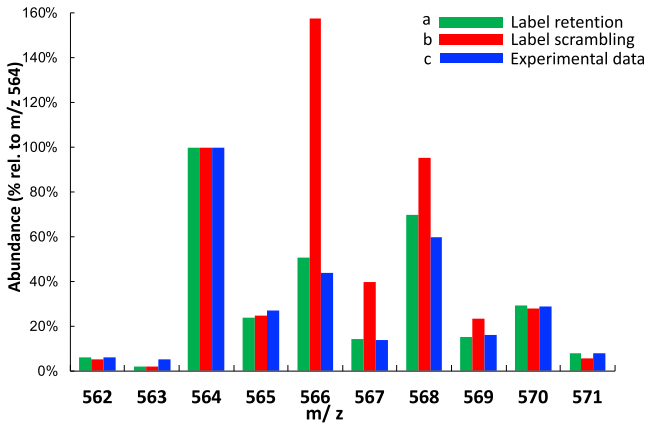

Figure 8. Theoretical and experimental ion abundances for the mass spectrum in the $[M + 2O]^+$ region from the reaction of **Ni**(μ-S_{PhNMe2})(μ-S'_{N2})**Fe** with a 62:38 mixture of $^{16}O_2/^{18}O_2$ (a) by label retention; (b) by label scrambling; and (c) the experimental results.

DOI: 10.1021/jacs.9b07448
J. Am. Chem. Soc. 2019, 141, 15338−15347

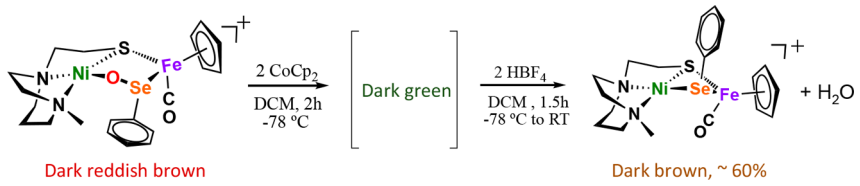

Figure 9. Oxygen removal reaction using Cp_2Co as reductant and HBF_4.

oxygens on sulfur are from one oxygen molecule. This agrees with previous studies on monomeric NiN_2S_2 complexes featuring terminal *cis*-dithiolates, Figure 1, that have shown that the addition of $^3\Sigma$ O_2 proceeds primarily through a concerted mechanism to produce both bissulfenates (RSO^-) as well as mono- and bissulfinates (RSO_2).[35,38]

Oxygenated Chalcogenide Repair. Earlier we determined that the O atom in the mono-oxy, μ-O, μ-E_{Ph}, complexes could be rapidly removed by PR_3 (R = Me or *o*-tolyl) in both the sulfur and selenium cases, regaining the μ-E_{Ph}.[41] However, electrochemical reductions in the presence of acid were ineffective toward removal of the O atom as H_2O. In the current study, Cp_2Co was adopted as an electron source and HBF_4 as proton source. A dark reddish-brown CH_2Cl_2 solution of Ni−O−Se_{PhH}-Fe, with ν(CO) 1954 cm^{-1}, was cooled to −78 °C and transferred into a precooled flask containing 2 equiv of Cp_2Co powder whereupon a reduced, dark green, CO-containing species of unknown composition was formed, Figure 9. On subsequent addition of 2 equiv of HBF_4, a gradual color change back to dark brown was observed over 1.5 h, along with a shift in the ν(CO) to 1934 cm^{-1}, indicating O atom removal and a spectroscopic yield of 60%. The $^+$ESI-mass spectrum confirmed the deoxygenation and return to **Ni**(μ-Se_{PhH})(μ-S'_{N2})**Fe**. Infrared and proton NMR spectroscopies indicated that the oxygen was removed as H_2O. An experiment with the one-oxy-sulfur analogue, Ni−O−S_{PhH}−Fe as a mixture with the two-oxy species, indicated reduction of the former; however, the sulfinato species was not affected. Addition of excess Cp_2Co resulted in overall degradation/decomposition.

To further examine the O removal from the sulfinate, we took the isolated two-oxy species or sulfinato complex, Ni−O−S(=O)Fe, in the case of X = NMe_2 and attempted the "repair" using Cp_2Co and HBF_4. After adding Cp_2Co, the intensity of ν(CO) 1960 cm^{-1} decreased, but no new band was observed even after 6 h, or with increased amounts of HBF_4. Further analysis of the $^+$ESI-mass spectrum indicates a low intensity signal at m/z 564 for the two-oxy species, but no indication of the reduced species, either one-oxy or the NiSFe parent complex.

The model repair process shown in Figure 9 is of relevance to the soluble, NAD^+-reducing [NiFe]-H_2ase from *R. eutropha*, whose S-oxygenated active site has been suggested to be reversible under O_2 and $NADH/H^+$.[28,52] In the proposed mechanism for the latter, the S-mono-oxygenate is reduced by NADH; with added H^+ producing H_2O. Similarly, in our repair process, the reductant Cp_2Co analogous to NADH, and along with the H^+, removes the O atom as H_2O.

CONCLUSIONS AND FINAL REMARKS

The salient features of this study follow:

(a) The nominal models of [NiFeS]- and [NiFeSe]-H_2ase active sites described above with bridging chalcogenides function as a probe of O_2 reactivity that yield isolable NiFe complexes where thiolate and selenolate are converted into sulf- and seleno-oxygenates. The presence of a carbon monoxide reporter ligand on Fe offered opportunity to explore "electronic alchemy" through remote effects of substituents on the E_{PhX} ligand that effectively (electronically) transformed S into Se. Preliminary Mossbauer studies find simple quadrupole doublets and nearly identical isomer shifts for the parent Ni−Fe−S and Ni−Fe−Se reduced complexes. Thus, the increased electron density from the Se that influences the ν(CO) IR values via Fe^{II} has no effect on the iron nuclei.

(b) The stability of these NiFe complexes, even under siege by O_2, is impressive. Crystallography finds only minimal changes in the coordination sphere of the bimetallic complex; the NiFe core is maintained with marginal differences in the Ni···Fe distances even though the -E_{PhX} bridging ligand has been expanded into an Ni−O−S−Fe or Ni−O−Se−Fe unit.

(c) Supported by earlier DFT computations,[41] we surmise that the rigidity of the tridentate N_2S "pincer"-type ligand guides production of E-oxygenates at the more mobile, monodentate, bridging E_{PhX} ligand site. Consistent with this conclusion are results from the Ogo group using NiN_2S_2 (with N_2S_2 as a fixed tetradentate binding site for Ni^{II}) as metalloligand to Cp^*Fe^{II}, bearing an open site on iron.[48−50] Under O_2, such Ni−Fe complexes yield isolable Fe^{IV}(peroxo) species, with O_2^{2-} side-on bound to Fe in [NiN_2S_2−Fe(O_2)Cp^*]$^+$ rather than any of the S-oxygenates displayed in Figure 1.

(d) The oxidation states of Ni and Fe in the product oxygenates of our study remain at Ni^{II} and Fe^{II} for both the selenium and the sulfur derivatives. However, we note that low temperature (0 °C) monitors of the O_2 reactions with the Ni−Fe containing the μ-S_{PhNMe2} bridging ligand found a buildup of a transient (but long-lived) EPR-active species as the reaction proceeded; a signal at $g_{avg} \approx 2.09$ is assigned to Ni^{III}, while one at g = 4.19 is likely Fe^{III}, see Supporting Information (Figures S60−S62). At reaction's end, oxygenated sulfurs were produced and the (presumed) Ni^{III} signal had disappeared. Some byproduct containing iron(III) is found in the oxidized residue from these reactions. These observations are reminiscent of the early EPR studies of [NiFe]-H_2ase redox poised in different levels, which gave rise to signals for Ni-A and Ni-B.[1,26,27]

(e) The preference of O atom-bridged S and Ni, that we observed here, is seen in the sulfenato complex of O-damaged [NiFeS]-H_2ase (Figure 1). The Ni−O−Se−Fe as a bridging unit is also observed here, but it is opposite to the Ni−Se−O−Fe arrangement found in one of the forms of O-damaged [NiFeSe]-H_2ase.[30,31] In fact, protein crystallography has uncovered a variety of chalcogen-oxgenates and myriad binding modes in the structures of oxygen-damaged [NiFe]-H_2ase enzyme active sites; such a display is likely a benefit of reaction within a restrictive enzyme active site cavity that partially accounts for the

DOI: 10.1021/jacs.9b07448
J. Am. Chem. Soc. 2019, 141, 15338−15347

longevity of these species. In contrast, in oxygenated solutions containing our small molecule active-site analogues, serious oxygen exposure and damage is likely to lead to intractable metal oxides.

(f) While there are discernible variations in oxygen uptake and product distributions that show correlations with electronic differences in the para-substituent series, the possible causes are many and expected to be intricately interrelated. For example, enhancement of electron-rich character at E in E_{PhX} from the para-substituent effect increases the likelihood for O_2 binding both to E, S or Se, as well as to the metals with which they bridge. Assuming that the affinity for the E_{PhX} ligand by Fe^{II} continues to be greater than to the Ni^{II}, then the O_2-uptake activity should be limited to the two sites, Ni^{II} and -E_{PhX}. Whether the O_2 activation by Ni precedes O atom attachment to E is unknown at this point; whether the mono-oxy species result from an initial dioxy species in all cases is also unclear. A full computational mechanistic study will address such questions.

We have seen in these studies, consistent with the enzyme studies or results, that compared to sulfur in nearly identical chemical environment, selenium exhibits more facility for O_2 uptake.[17] The observed oxygenated Se product is a single oxy species (we cannot discount a dioxy species as intermediate), and O atom removal is facile for selenium. Excellent commentaries regarding "Why nature chose..."[17,51] heavier elements in the chalcogen or pnictogen family for numerous biological processes clearly point to their intricate interactions with oxygen. In hydrogenase enzyme chemistry, the many benefits of selenium incorporation include not only enhancement of catalytic activity through proton shuttling and hydrogen expulsion rates but also of protection of the active sites from poisonous O_2. Such benefits apparently outweigh the added cost to the organism of the biosynthesis. As of now, there are few synthetic HER or ORR molecular catalysts[2] that target selenium substitution and explore possible paybacks for the minimal synthetic expenditure. We hope that our results point to new directions in this regard.

■ ASSOCIATED CONTENT

Supporting Information

The Supporting Information is available free of charge on the ACS Publications website at DOI: 10.1021/jacs.9b07448.

Experimental details, characterizations, additional spectroscopic, preliminary Mössbauer and EPR studies, and computational details (PDF)

X-ray crystallographic data for 1934935 (CIF), 1934963 (CIF), 1934974 (CIF), 1934976 (CIF), 1934979 (CIF), and 1934980 (CIF)

■ AUTHOR INFORMATION

Corresponding Author

*marcetta@mail.chem.tamu.edu

ORCID

Xuemei Yang: 0000-0001-8069-5831
Lindy C. Elrod: 0000-0002-5583-2731
Trung Le: 0000-0003-3913-8966
Michael B. Hall: 0000-0003-3263-3219
Marcetta Y. Darensbourg: 0000-0002-0070-2075

Notes

The authors declare no competing financial interest.

■ ACKNOWLEDGMENTS

This work was financially supported by the National Science Foundation (CHE-1300787, CHE-1664866 to M.B.H. and CHE-1665258 to M.Y.D.) and the Robert A. Welch Foundation (A-0648 to M.B.H. and A-0924 to M.Y.D.). We thank Kyle Burns, Waseem Vali, and Prof. Paul Lindahl for the preliminary Mössbauer studies.

■ REFERENCES

(1) Cammack, R.; Frey, M.; Robson, R. *Hydrogen as a Fuel*; Taylor and Francis: London, 2001.

(2) Vincent, K. A.; Parkin, A.; Lenz, O.; Albracht, S. P. J.; Fontecilla-Camps, J. C.; Cammack, R.; Friedrich, B.; Armstrong, F. A. Electrochemical Definitions of O_2 Sensitivity and Oxidative Inactivation in Hydrogenases. *J. Am. Chem. Soc.* **2005**, *127*, 18179−18189.

(3) Wakerley, D. W.; Reisner, E. Oxygen-tolerant Proton Reduction Catalysis: Much O_2 about Nothing? *Energy Environ. Sci.* **2015**, *8*, 2283−2295.

(4) Buhrke, T.; Lenz, O.; Krauss, N.; Friedrich, B. Oxygen Tolerance of the H_2-sensing [NiFe] Hdrogenase from *Ralstonia eutropha* H16 Is Based on Limited Access of Oxgen to the Active Site. *J. Biol. Chem.* **2005**, *280*, 23791−23796.

(5) Duche, O.; Elsen, S.; Cournac, L.; Colbeau, A. Enlarging the Gas Access Channel to the Active Site Renders the Regulatory Hydrogenase HupUV of *Rhodobacter Capsulatus* O_2 Sensitive Without Affecting Its Transductory Activity. *FEBS J.* **2005**, *272*, 3899−3908.

(6) Fritsch, J.; Lenz, O.; Friedrich, B. Structure, Function and Biosynthesis of O_2-tolerant Hydrogenases. *Nat. Rev. Microbiol.* **2013**, *11*, 106−114.

(7) Lenz, O.; Ludwig, M.; Schubert, T.; Burstel, I.; Ganskow, S.; Goris, T.; Schwarze, A.; Friedrich, B. H_2 Conversion in the Presence of O_2 as Performed by the Membrane-Bound [NiFe]-Hydrogenase of *Ralstonia eutropha*. *ChemPhysChem* **2010**, *11*, 1107−1119.

(8) Lubitz, W.; Ogata, H.; Rudiger, O.; Reijerse, E. *Chem. Rev.* **2014**, *114*, 4081−4148.

(9) Pandelia, M.-E.; Fourmond, V.; Tron-Infossi, P.; Lojou, E.; Bertrand, P.; Léger, C.; Giudici-Orticoni, M.-T.; Lubitz, W. Membrane-Bound Hydrogenase I from the Hperthermophilic Bacterium *Aquifex aeolicus*: Enzyme Activation, Redox Intermediates and Oxygen Tolerance. *J. Am. Chem. Soc.* **2010**, *132*, 6991−7004.

(10) Shomura, Y.; Yoon, K. S.; Nishihara, H.; Higuchi, Y. Structural Basis for a [4Fe-3S] Cluster in the Oxygen-tolerant Membrane-bound [NiFe]-hydrogenase. *Nature* **2011**, *479*, 253−256.

(11) Volbeda, A.; Amara, P.; Darnault, C.; Mouesca, J. M.; Parkin, A.; Roessler, M. M.; Armstrong, F. A.; Fontecilla-Camps, J. C. X-rayCrystallographic and Computational Studies of the O_2-tolerant [NiFe]-hydrogenase 1 from *Escherichia coli*. *Proc. Natl. Acad. Sci. U. S. A.* **2012**, *109*, 5305−5310.

(12) Baltazar, C. S. A.; Marques, M. C.; Soares, C. M.; DeLacey, A. M.; Pereira, I. A. C.; Matias, P. M. Nickel-Iron-Selenium Hydrogenases - An Overview. *Eur. J. Inorg. Chem.* **2011**, *2011*, 948−962.

(13) De Lacey, A. L.; Gutierrez-Sanchez, C.; Fernandez, V. M.; Pacheco, I.; Pereira, I. A. FTIR Spectroelectrochemical Characterization of the Ni-Fe-Se Hydrogenase from *Desulfovibrio vulgaris* Hildenborough. *JBIC, J. Biol. Inorg. Chem.* **2008**, *13*, 1315−1320.

(14) Parkin, A.; Goldet, G.; Cavazza, C.; Fontecilla-Camps, J. C.; Armstrong, F. A. The Difference a Se Makes? Oxygen-Tolerant Hydrogen Production by the [NiFeSe]-Hydrogenase from *Desulfomicrobium baculatum*. *J. Am. Chem. Soc.* **2008**, *130*, 13410−13416.

(15) Wombwell, C.; Caputo, C. A.; Reisner, E. [NiFeSe]-Hydrogenase Chemistry. *Acc. Chem. Res.* **2015**, *48*, 2858−2865.

(16) Garcin, E.; Vernede, X.; Hatchikian, E.; Volbeda, A.; Frey, M.; Fontecilla-Camps, J. The Crystal Structure of a Reduced [NiFeSe] Hydrogenase Provides an Image of the Activated Catalytica Center. *Structure* **1999**, *7*, 557−566.

DOI: 10.1021/jacs.9b07448
J. Am. Chem. Soc. 2019, 141, 15338−15347

(17) Reich, H. J.; Hondal, R. J. Why Nature Chose Selenium. *ACS Chem. Biol.* **2016**, *11*, 821−841.
(18) Wombwell, C.; Reisner, E. Synthesis, Structure and Reactivity of Ni Site Models of [NiFeSe] Hydrogenases. *Dalton Trans* **2014**, *43*, 4483−4493.
(19) (a) Wombwell, C.; Reisner, E. Synthetic Active Site Model of the [NiFeSe] Hydrogenase. *Chem. - Eur. J.* **2015**, *21*, 8096−8104. (b)) Marques, M. C.; Coelho, R.; De Lacey, A. L.; Pereira, I. A.C.; Matias, P. M. Redox State-dependent Changes in the Crystal Structure of [NiFeSe] Hydrogenase from *Desulfovibrio vulgaris Hildenborough*. *J. Mol. Biol.* **2010**, *396*, 893−907.
(20) Volbeda, A.; Martin, L.; Cavazza, C.; Matho, M.; Faber, B. W.; Roseboom, W.; Albracht, S. P. J.; Garcin, E.; Rousset, M.; Fontecilla-Camps, J. C. Structural Differences between the Ready and Unready Oxidized States of [NiFe] hydrogenases. *JBIC, J. Biol. Inorg. Chem.* **2005**, *10*, 239−249.
(21) Cracknell, J. A.; Wait, A. F.; Lenz, O.; Friedrich, B.; Armstrong, F. A. A Kinetic and Thermodynamic Understanding of O_2 Tolerance in [NiFe]-hydrogenases. *Proc. Natl. Acad. Sci. U. S. A.* **2009**, *106*, 20681−20686.
(22) Jones, A. K.; Lamle, S. E.; Pershad, H. R.; Vincent, K. A.; Albracht, S. P. J.; Armstrong, F. A. Enzyme Electrokinetics: Electrochemical Studies of the Anaerobic Interconversions between Active and Inactive States of *Allochromatium vinosum* [NiFe]-hydrogenase. *J. Am. Chem. Soc.* **2003**, *125*, 8505−8514.
(23) Lamle, S. E.; Albracht, S. P.; Armstrong, F. A. The Mechanism of Activation of a [NiFe]-Hydrogenase by Electrons, Hydrogen, and Carbon Monoxide. *J. Am. Chem. Soc.* **2005**, *127*, 6595−6604.
(24) Radu, V.; Frielingsdorf, S.; Lenz, O.; Jeuken, L. J. Reactivation from the Ni-B State in [NiFe] Hydrogenase of *Ralstonia eutropha* is Controlled by Reduction of the Superoxidised Proximal Cluster. *Chem. Commun.* **2016**, *52*, 2632−2635.
(25) Armstrong, F. A.; Belsey, N. A.; Cracknell, J. A.; Goldet, G.; Parkin, A.; Reisner, E.; Vincent, K. A.; Wait, A. F. Dynamic Electrochemical Investigations of Hydrogen Oxidation and Production by Enzymes and Implications for Future Technology. *Chem. Soc. Rev.* **2009**, *38*, 36−51.
(26) Albracht, S. P. J.; Graf, E. G.; Thauer, R. K. The EPR Properties of Nickel in Hydrogenase from *Methanobacterium thermoautotrophicum*. *FEBS Lett.* **1982**, *140*, 311−313.
(27) Flores, M.; Agrawal, A. G.; van Gastel, M.; Gartner, W.; Lubitz, W. Electron-Electron Double Resonance-Detected NMR to Measure Metal Hyperfine Interactions: ^{61}Ni in the Ni-B State of the [NiFe] Hydrogenase of *Desulfovibrio Vulgaris* Miyazaki F. *J. Am. Chem. Soc.* **2008**, *130*, 2402−2403.
(28) Horch, M.; Lauterbach, L.; Mroginski, M. A.; Hildebrandt, P.; Lenz, O.; Zebger, I. Reversible Active Site Sulfoxygenation Can Explain the Oxygen Tolerance of a NAD^+-Reducing [NiFe] Hydrogenase and Its Unusual Infrared Spectroscopic Properties. *J. Am. Chem. Soc.* **2015**, *137*, 2555−2564.
(29) Volbeda, A.; Martin, L.; Barbier, E.; Gutiérrez-Sanz, O.; DeLacey, A. L.; Liebgott, P.; Dementin, S.; Rousset, M.; Fontecilla-Camps, J. C. Crystallographic Studies of [NiFe]-hydrogenase Mutants: towards Consensus Structures for the Elusive Unready Oxidized States. *JBIC, J. Biol. Inorg. Chem.* **2015**, *20*, 11−22.
(30) Marques, M. C.; Coelho, R.; De Lacey, A. L.; Pereira, I. A. C.; Matias, P. M. The Three-Dimensional Structure of [NiFeSe] Hydrogenase from *Desulfovibrio vulgaris* Hildenborough: A Hydrogenase without a Bridging Ligand in the Active Site in Its Oxidised, "as-Isolated" State. *J. Mol. Biol.* **2010**, *396*, 893−907.
(31) Volbeda, A.; Amara, P.; Iannello, M.; De Lacey, A. L.; Cavazza, C.; Fontecilla-Camps, J. C. Structural Foundations for the O_2 Resistance of *Desulfomicrobium baculatum* [NiFeSe]-hydrogenase. *Chem. Commun.* **2013**, *49*, 7061−7063.
(32) Teixeira, M.; Fauque, G.; Moura, I.; Lespinat, P. A.; Berlier, Y.; Prickril, B.; Peck, H. D.; Xavier, A. V.; Gall, J. L.; Moura, J. J. G. Nickel-[iron-sulfur]-selenium-containing Hydrogenases from *Desulfovibrio baculatus* (DSM 1743). *Eur. J. Biochem.* **1987**, *167*, 47−58.
(33) Marques, M. C.; Tapia, C.; Gutierrez-Sanz, O.; Ramos, A. R.; Keller, K. L.; Wall, J. D.; De Lacey, A. L.; Matias, P. M.; Pereira, I. A. C. The Direct Role of Selenocysteine in [NiFeSe] Hydrogenase Maturation and Catalysis. *Nat. Chem. Biol.* **2017**, *13*, 544−550.
(34) Grapperhaus, C. A.; Maguire, M. J.; Tuntulani, T.; Darensbourg, M. Y. Singlet Oxygen and the Production of Sulfur Oxygenates of Nickel(II) and Palladium(II) Thiolates. *Inorg. Chem.* **1997**, *36*, 1860−1866.
(35) Farmer, P. J.; Solouki, T.; Mills, D. K.; Soma, T.; Russell, D. H.; Reibenspies, J. H.; Darensbourg, M. Y. Isotopic Labeling Investigation of Oxygenation of Nickel-Bound Thiolates by Molecular Oxygen. *J. Am. Chem. Soc.* **1992**, *114*, 4601−4605.
(36) Grapperhaus, C. A.; Darensbourg, M. Y. Oxgen Capture by Sulfur in Nickel Thiolates. *Acc. Chem. Res.* **1998**, *31*, 451−459.
(37) Grapperhaus, C. A.; Darensbourg, M. Y.; Sumner, L. W.; Russell, D. H. Template Effect for O_2 Addition across cis-Sulfur Sites in Nickel Dithiolates. *J. Am. Chem. Soc.* **1996**, *118*, 1791−1792.
(38) Farmer, P. J.; Solouki, T.; Soma, T.; Russell, D. H.; Darensbourg, M. Y. Divergent Pathways for the Addition of Dioxygen to Sulfur in Nickel cis-Dithiolates: An Isotopomeric Analysis. *Inorg. Chem.* **1993**, *32*, 4171−4172.
(39) Lindenmaier, N. J.; Wahlefeld, S.; Bill, E.; Szilvasi, T.; Eberle, C.; Yao, S.; Hildebrandt, P.; Horch, M.; Zebger, I.; Driess, M. An S-oxygenated [NiFe] Complex Modelling Sulfenate Intermediates of an O_2-Tolerant Hydrogenase. *Angew. Chem., Int. Ed.* **2017**, *56*, 2208−2211.
(40) Choudhury, S. B.; Pressler, M. A.; Mirza, S. A.; Day, R. O.; Maroney, M. J. Structure and Redox Chemistry of Analogous Nickel Thiolato and Selenolato Complexes: Implications for the Nickel Sites in Hydrogenase. *Inorg. Chem.* **1994**, *33*, 4831−4839.
(41) Yang, X.; Elrod, L. C.; Reibenspies, J. H.; Hall, M. B.; Darensbourg, M. Y. Oxygen Uptake in Complexes Related to [NiFeS]- and [NiFeSe]- hydrogenase Active Sites. *Chem. Sci.* **2019**, *10*, 1368−1373.
(42) Broering, E. P.; Dillon, S.; Gale, E. M.; Steiner, R. A.; Telser, J.; Brunold, T. C.; Harrop, T. C. Accessing Ni(III)-Thiolate Versus Ni(II)-Thiyl Bonding in a Family of Ni-N_2S_2 Synthetic Models of NiSOD. *Inorg. Chem.* **2015**, *54*, 3815−3828.
(43) Jenkins, R. M.; Singleton, M. L.; Leamer, L. A.; Reibenspies, J. H.; Darensbourg, M. Y. Orientation and Stereodynamic Paths of Planar Monodentate Ligands in Square Planar Nickel N_2S complexes. *Inorg. Chem.* **2010**, *49*, 5503−5514.
(44) Hammett, L. P. The Effect of Structure upon the Reactions of Organic Compounds Benzene Derivatives. *J. Am. Chem. Soc.* **1937**, *59*, 96−103.
(45) Frisch, M. J.; Trucks, G. W.; Schlegel, H. B.; Scuseria, G. E.; Robb, M. A.; Cheeseman, J. R.; Scalmani, G.; Barone, V.; Mennucci, B.; Petersson, G. A.; Nakatsuji, H.; Caricato, M.; Li, X.; Hratchian, H. P.; Izmaylov, A. F.; Bloino, J.; Zheng, G.; Sonnenberg, J. L.; Hada, M.; Ehara, M.; Toyota, K.; Fukuda, R.; Hasegawa, J.; Ishida, M.; Nakajima, T.; Honda, Y.; Kitao, O.; Nakai, H.; Vreven, T.; Montgomery, J. A., Jr.; Peralta, J. E.; Ogliaro, F.; Bearpark, M.; Heyd, J. J.; Brothers, E.; Kudin, K. N.; Staroverov, V. N.; Kobayashi, R.; Normand, J.; Raghavachari, K.; Rendell, A.; Burant, J. C.; Iyengar, S. S.; Tomasi, J.; Cossi, M.; Rega, N.; Millam, J. M.; Klene, M.; Knox, J. E.; Cross, J. B.; Bakken, V.; Adamo, C.; Jaramillo, J.; Gomperts, R.; Stratmann, R. E.; Yazyev, O.; Austin, A. J.; Cammi, R.; Pomelli, C.; Ochterski, J. W.; Martin, R. L.; Morokuma, K.; Zakrzewski, V. G.; Voth, G. A.; Salvador, P.; Dannenberg, J. J.; Dapprich, S.; Daniels, A. D.; Farkas, O.; Foresman, J. B.; Ortiz, J. V.; Cioslowski, J.; Fox, D. J. *Gaussian 16*; Gaussian, Inc.: Wallingford, CT, 2016.
(46) *AMPAC 9*; Semichem Inc.: Shawnee, KS, 2008.
(47) Glendening, E. D.; Badenhoop, J. K.; Reed, A. E.; Carpenter, J. E.; Bohmann, J. A.; Morales, C. M.; Landis, C. R.; Weinhold, F. *NBO 6.0*; Theoretical Chemistry Institute, University of Wisconsin: Madison, WI, 2013.
(48) Isegawa, M.; Sharma, A. K.; Ogo, S.; Morokuma, K. DFT Study on Fe(IV)-Peroxo Formation and H Atom Transfer Triggered O2 Activation by NiFe Complex. *Organometallics* **2018**, *37*, 1534−1545.

DOI: 10.1021/jacs.9b07448
J. Am. Chem. Soc. 2019, 141, 15338−15347

(49) Ogo, S. H_2 and O_2 Activation- A Remarkable Insight into Hydrogenase. *Chem. Rec.* **2014**, *14*, 397−409.
(50) Ogo, S. H_2 and O_2 Activation by [NiFe]hydrogenase -Insights from model complexes. *Coord. Chem. Rev.* **2017**, *334*, 43−53.
(51) Westheimer, F. H. Why Nature Chose Phosphates. *Science* **1987**, *235*, 1173−1178.
(52) Lauterbach, L.; Lenz, O. Catalytic Production of Hydrogen Peroxide and Water by Oxygen- Tolerant [NiFe]-Hydrogenase during H_2 Cycling in the Presence of O_2. *J. Am. Chem. Soc.* **2013**, *135*, 17897−17905.

DOI: 10.1021/jacs.9b07448
J. Am. Chem. Soc. 2019, 141, 15338−15347